



Optimization schemes for selective molecular cleavage with tailored ultrashort laser pulses

Kevin Krieger^a, Alberto Castro^{b,*}, E.K.U. Gross^a

^aMax-Planck-Institut für Mikrostrukturphysik, Weinberg 2, D-06120 Halle, Germany

^bInstitute for Biocomputation and Physics of Complex Systems (BIFI), University of Zaragoza, E-50018 Zaragoza, Spain

ARTICLE INFO

Article history:

Available online 30 April 2011

Keywords:

Quantum optimal control theory
Time-dependent density-functional theory

ABSTRACT

We present some approaches to the computation of ultra-fast laser pulses capable of selectively breaking molecular bonds. The calculations are based on a mixed quantum-classical description: The electrons are treated quantum mechanically (making use of time-dependent density-functional theory), whereas the nuclei are treated classically. The temporal shape of the pulses is tailored to maximize a control target functional which is designed to produce the desired molecular cleavage. The precise definition of this functional is a crucial ingredient: we explore expressions based on the forces, on the momenta and on the velocities of the nuclei. The algorithm used to find the optimum pulse is also relevant; we test both direct gradient-free algorithms, as well as schemes based on formal optimal control theory. The tests are performed both on one dimensional models of atomic chains, and on first-principles descriptions of molecules.

© 2011 Elsevier B.V. All rights reserved.

1. Introduction

Soon after its first operation [1], the laser was expected to become the ultimate surgical tool at the nanoscopic level: Light, at convenient wave-lengths, monochromatic, coherent, and intense [2], was believed to open the avenue to selectively break (or create) molecular bonds. Unfortunately, the early attempts to perform this kind of photo-chemistry were only occasionally successful [3,4]. These attempts used “simple” monochromatic lasers, tinkering only with two parameters: the frequency and the intensity. However, the energy, tuned to a particular vibrational frequency and initially deposited on the corresponding bond, is soon re-distributed to the rest of the modes, and produces undesired global heating instead of selective cleavage [5].

The “controlled” laser assisted photo-chemistry advanced along with improvements on laser technology, with methodologies such as the control of quantum interference proposed by Brumer and Shapiro [6–8], the “pump-dump” control proposed by Tannor and Rice [9,10], stimulated Raman adiabatic passage [11], wave-packet interferometry [12], and others [13,14]. The key ingredients, beyond mere mono-chromaticity and intensity, were shown to be coherence (and therefore, interference), detailed shaping, and ultra-short pulse duration (in the femto-second time scale). The most successful technique is adaptive feedback control (AFC), as proposed by Judson and Rabitz [15], and first realized in 1997 [16].

There are two important components in an AFC experiment: the pulse shaper [17], and the search algorithm fed by the repeated measurement outcome. The former is an instrument that allows to almost arbitrarily design laser pulses. The increasing versatility of modern laser sources (regarding pulse length, power, and accessible frequencies), and the capacity of pulse shapers to modify the produced pulses, set the boundaries that theoretical studies such as the one presented in this work must respect; however these boundaries are rapidly pushed further, allowing more versatile pulses.

Quantum optimal control theory (QOCT) [18–21] is the most general theoretical framework aimed to the prediction of laser pulses that are optimal for a given task. It is the translation to the quantum realm of a very broad mathematical area, optimal control, that is best formulated in the language of systems theory [22,23]. Its use for quantum processes was initiated in the 80s [19–21] – responding to the initial experimental stir. In some way, QOCT encompasses all the previously mentioned optimization methods (in as much as it may describe them theoretically). The theory is constructed on top of some chosen level of approximation for the description of the process that is to be optimized. Here lies the main limitation of QOCT: [14] it may only be predictive if the system is simple enough to allow for an accurate approximation of its evolution. In most cases, however, the process is too complex.

If some reliable predictive power is to be expected from any QOCT calculation, one should attempt a first-principles description. In particular, in the regime of interest, the dynamics of the electrons should be carefully treated: high intensity electric fields at

* Corresponding author.

E-mail address: acastro@bifi.es (A. Castro).

high frequencies affect directly the electronic degrees of freedom. Indeed, when many-electron systems are irradiated with strong femtosecond pulses a number of interesting non-trivial photo-reactions may take place: above-threshold or tunnel ionization, bond hardening or softening, high harmonic generation, photo-isomerization, photo-fragmentation, Coulomb explosion, etc. [24–26]. Yet most of the computational work until now has relied on simplified models, and has usually worked with nuclear wave packets – defined on a few relevant reaction variables, after a reduction of dimensionality has been postulated – moving on one or a few Born–Oppenheimer potential energy surfaces, and therefore mostly ignoring the dynamic behavior of the electrons. Direct, first-principles, electronic control has been scarcely attempted [27], unless for one-electron cases [28–30].

One viable alternative to treat electronic motion in an ab initio way is time-dependent density-functional theory (TDDFT) [31,32]. Recently some of us have demonstrated the feasibility of performing QOCT with TDDFT [33]. This was not obvious due to the non-linear character of the TDDFT equations: the usual QOCT equations assume a standard, linear Schrödinger-like evolution, and the resulting QOCT equations are correspondingly simple. However, the presence of the Hartree, exchange and correlation term in the TDDFT equations need special care.

TDDFT offers reasonable accuracy when dealing with the non-linear response of molecular systems, with a fraction of the cost of methods based on the wave function. Furthermore, the electronic system described within TDDFT may then be coupled to the ionic motion in a mixed quantum–classical description [34–37]. This model will obviously ignore quantum nuclear effects, but may be sufficient for the description of many processes. In this work we present our first results based on this combination. In Section 2, the essential equations are displayed, as well as a brief description of the numerical procedure. Section 3 describes the results of the optimizations when the target functional is defined in terms of the values of the forces on the nuclei at the end of the laser pulse, for 1D models, whereas in Section 4, the target functional is defined in terms of the momenta. In Section 5, the attempt to selectively break molecular chains is described. Finally, Sections 6 and 7 display results for fully ab initio 3D calculations.

2. Methodology

2.1. Essentials of QOCT

We consider a quantum mechanical system governed by Schrödinger's equation during the time interval $[0, T]$ (atomic units will be used hereafter):

$$i \frac{\partial \Psi}{\partial t}(x, t) = \hat{H}[u, t] \Psi(x, t), \quad (1)$$

$$\Psi(x, 0) = \Psi_0(x), \quad (2)$$

where x is the full set of quantum coordinates, and u is a control, typically a set of parameters that determine the precise shape of an external potential applied to the system. Mathematically, we can distinguish two types of “representation” for the control u :

1. u is a real valued continuous function defined on the time interval of interest (the control function); we will call this a “real-time” representation of the control. For example, the Hamiltonian may have the form:

$$\hat{H}[u, t] = \hat{H}_0 + u(t)\hat{D}. \quad (3)$$

2. u is a set of N real parameters that modifies the precise shape of the Hamiltonian; typically, this set of parameters fixes the form of a control function; we will call this a “parameterized” representation of the control.

In any case, the specification of u , together with an initial value condition, $\Psi(0) = \Psi_0$ determines the full evolution of the system, $\Psi[u]$, via the propagation of Schrödinger's equation.

We wish to maximize the function G ,

$$G[u] = F[\Psi[u], u], \quad (4)$$

where F is the so-called “target functional”; in many cases it is split into two parts, $F[\Psi, u] = J_1[\Psi] + J_2[u]$, so that J_1 only depends on the state of the system, and J_2 is called the “penalty”, and depends explicitly on the control u . An important distinction should be made regarding J_1 :

1. It may depend on the full evolution of the system during the time interval $[0, T]$; this is usually called a time-dependent target. We may write this as $J_1[\Psi] = J_1^{[0, T]}[\Psi]$, where the $J_1^{[0, T]}[\Psi]$ functional admits continuous functional derivatives, in particular $\frac{\delta J_1^{[0, T]}}{\delta \Psi^*(x, t)}$ is continuous at $t = T$.
2. J_1 may only depend on the state of the system at the end of the propagation, which we may write as $J_1[\Psi] = J_1^T[\Psi(T)]$.

Of course, J_1 may be defined as a combination of the two options, i.e.:

$$J_1[\Psi] = J_1^{[0, T]}[\Psi] + J_1^T[\Psi(T)]. \quad (5)$$

Note that, in this case:

$$\frac{\delta J_1}{\delta \Psi^*(x, t)} = \frac{\delta J_1^{[0, T]}}{\delta \Psi^*(x, t)} + \delta(t - T) \frac{\delta J_1^T}{\delta \Psi^*(x, T)}. \quad (6)$$

In most cases these functionals are defined as the expectation value of some observable \hat{O} . For example:

$$J_1^T[\Psi(T)] = \langle \Psi(T) | \hat{O} | \Psi(T) \rangle \text{ or:} \quad (7)$$

$$J_1^{[0, T]}[\Psi(T)] = \int_0^T dt \langle \Psi(t) | \hat{O}(t) | \Psi(t) \rangle. \quad (8)$$

One needs now an optimization algorithm to find the maximum (or maxima) of G . Two broad families can be distinguished: gradient-free procedures, that only require some means to compute the value of G given a control input u , and gradient-based procedures, that also necessitate the computation of the gradient of G with respect to u (more precisely, the functional derivative if u is a continuous function in time). We will not repeat here a derivation that can be found elsewhere in several forms [20,21,38,39]; the key equations are:

$$\nabla_u G[u] = \nabla_u F[\Psi, u]_{\Psi=\Psi[u]} + 2\text{Im} \int_0^T dt \langle \chi[u](t) | \nabla_u \hat{H}[u, t] | \Psi[u](t) \rangle, \quad (9)$$

in case u is a set of real parameters, and:

$$\frac{\delta G}{\delta u(t)} = \frac{\delta F[\Psi, u]}{\delta u(t)}_{\Psi=\Psi[u]} + 2\text{Im} \langle \chi[u](t) | \hat{D} | \Psi[u](t) \rangle, \quad (10)$$

if u is a function in time, and the Hamiltonian is given by Eq. (3).

Note that a new “wave function”, $\chi[u]$, has been introduced; it is given by the solution of:

$$i \frac{\partial \chi[u]}{\partial t}(x, t) = \hat{H}^\dagger[u, t] \chi[u](x, t) - i \frac{\delta J_1^{[0, T]}}{\delta \Psi^*[u](x, t)}, \quad (11)$$

$$\chi[u](x, T) = \frac{\delta J_1^T}{\delta \Psi^*[u](x, T)}. \quad (12)$$

This is similar to the original Schrödinger's equation (Eqs. (1) and (2)), except: (1) It may be inhomogeneous, if $J_1^{[0, T]}$ is not zero (i.e. if the target is time-dependent [38,39]), and (2) The initial condition is given at the final time $t = T$, which implies it must be propagated backwards.

The computation of the gradient or functional derivative of G , therefore, requires $\mathcal{Y}[u]$ and $\chi[u]$, which are obtained by first propagating Eq. (1) forwards, and then Eq. (11) backwards. The maxima of G are found at the critical points $\nabla_u G[u] = 0$ or $\frac{\delta G}{\delta u(t)} = 0$; in order to arrive to these maxima one can use a variety of algorithms, some of which are listed in Section 2.3.2.

2.2. Mixed quantum–classical description with TDDFT

Instead of solving the many-electron Schrödinger equation, TDDFT allows to work with a set of one-electron equations, the Kohn–Sham (KS) system, corresponding to a fictitious system whose one-particle density is by construction identical to that of the real one:

$$i \frac{\partial \varphi_i}{\partial t}(\vec{r}, t) = -\frac{1}{2} \nabla^2 \varphi_i(\vec{r}, t) + [v_{\text{ext}}(\vec{r}, t) + v_{\text{Hartree}}[n_t](\vec{r}) + v_{\text{xc}}[n](\vec{r}, t)] \varphi_i(\vec{r}, t), \quad (13)$$

$$n(\vec{r}, t) = \sum_{i=1}^N 2 |\varphi_i(\vec{r}, t)|^2 \equiv n_t(\vec{r}). \quad (14)$$

We will assume a system with $2N$ electrons in a spin compensated configuration, evolving in a spin independent Hamiltonian. This means N doubly occupied KS orbitals $\varphi_i, i = 1, \dots, N$. The system evolves on an external time-dependent potential v_{ext} , that may include the interaction with a set of nuclei, as well as external electric fields. The Hartree term v_{Hartree} is the classic electrostatic potential, and the rest of the electron–electron interaction is encoded in the exchange and correlation potential v_{xc} . In this work, we will only use the adiabatic extension of the local density approximation (LDA) [40], although the extension to other more sophisticated schemes is straightforward.

The external potential can depend on a control function, and therefore control theory can be employed to find optimal evolutions of the KS system. Note, however, that the KS equations are not akin to the conventional Schrödinger equation, since they are non-linear. The QOCT expressions presented above are therefore not valid; the correct equations have been presented elsewhere [33]; however, in this work we will either (1) take the independent electron approximation, which amounts to ignoring the mentioned non-linearity, for model calculations, or (2) utilize a gradient-free version of QOCT, for which we can use the full-fledged version of TDDFT.

In order to describe the combined coupled movement of electrons and (classical) nuclei, one can perform Ehrenfest dynamics on top of TDDFT [37]. The external term v_{ext} will couple the electrons to N_{nuc} nuclei located at positions $\vec{R}_\alpha(t)$ through an expression in the form:

$$v_{\text{ext}}(\vec{r}, t; \{\vec{R}_\beta(t)\}) = \sum_{\alpha=1}^{N_{\text{nuc}}} \frac{-Z_\alpha}{|\vec{R}_\alpha(t) - \vec{r}|} + \vec{E}(t) \cdot \vec{r}. \quad (15)$$

The evolution of the nuclear positions is then governed by an Ehrenfest equation in the form:

$$m_\alpha \frac{d^2}{dt^2} \vec{R}_\alpha(t) = \sum_{\beta=1}^{N_{\text{nuc}}} Z_\alpha Z_\beta \frac{\vec{R}_\alpha(t) - \vec{R}_\beta(t)}{|\vec{R}_\alpha(t) - \vec{R}_\beta(t)|^3} + Z_\alpha \vec{E}(t) - \int d^3m(\vec{r}, t) \nabla_{\vec{R}_\alpha} v_{\text{ext}}(\vec{r}, t; \{\vec{R}_\beta(t)\}). \quad (16)$$

2.3. Numerical implementation

All the ideas described above have been implemented in the `octopus` code. Since the numerical details of this platform are described elsewhere [41,42], here we will only list some essential

points. The laser field and the optimization algorithms are described below with more detail.

- Wave functions and densities are represented on a regular rectangular real space mesh. This is a suitable scheme to describe high intensity laser–electron interactions, since the electronic density visits regions in space far from the localized basis sets typically used in other schemes. Furthermore, the intrinsic locality allows for easy parallelization, and the only parameters controlling convergence are the grid spacing and the simulation box size.
- The electron–ion interaction is modelled with pseudopotentials. In this way, the Coulomb singularity is avoided, and the core electrons are removed from the calculation. For the first results described below, however, we will use 1D models, and the soft-Coulomb interaction to avoid singularities.
- The KS orbitals are evolved in real time with the help of a number of propagating algorithms [43]. This is crucial since all algorithms require multiple propagations.
- The code performs realistic 3D calculations, but it also allows 1D and 2D models, such as the ones we will present below.

2.3.1. The laser field

We will assume that laser pulses can be described in the dipole approximation, which is valid given the wave lengths and intensities that will be considered. In consequence, it suffices with an electric field in the form:

$$\vec{E}(t) = \epsilon(t) \vec{p}, \quad (17)$$

where \vec{p} is a unit vector that determines the polarization direction, and $\epsilon(t)$ determines the temporal dependence, and is the object to be optimized – i.e. the *control function*.

Not any function in time is admissible as a solution; there are physical and experimental constraints that must be respected. For example, an important physical constraint is:

$$\int_0^T dt \epsilon(t) = 0. \quad (18)$$

This condition follows from Maxwell's equations for a freely propagating pulse in the electric dipole approximation [44]. Also, the pulses must obviously start and end at zero:

$$\epsilon(0) = \epsilon(T) = 0. \quad (19)$$

It is important to reduce the search space to functions that are experimentally accessible, which means a limitation on the accessible frequency components, and on the intensities. Regarding the latter, usually it is done by considering the integrated intensity or *fluence*, defined as:

$$\mathcal{F}[\epsilon] = \int_0^T dt \epsilon^2(t). \quad (20)$$

Spectral constraints can also be imposed either by penalizing the undesired frequencies in the definition of the target [45], or by restricting from the start the search space to the correct subspace.

As discussed earlier, we may use a real-time representation, and therefore $\epsilon(t)$ is directly the control object u , or a parameterized representation, in which this control function $\epsilon(t)$ is determined by a set of parameters u . This distinction is relevant for the mathematical derivations (since in the former case functional derivatives must be used, whereas in the latter case one uses normal gradients). Numerically, however, a function in real time must also be discretized, and therefore the distinction disappears. Nevertheless, typically the number of degrees of freedom (number of grid points in time) will be much larger, and therefore the algorithms utilized will differ.

Regarding the choices for the parameterization, it is a natural choice to expand the control field in a basis set, and to establish the coefficients of this expansion as the parameters:

$$\epsilon(t) = \sum_{n=1}^N \tilde{\epsilon}_n g_n(t). \quad (21)$$

N is the dimension of the real basis set $\{g_n(t)\}$. It is chosen to be orthonormal over the interval $[0, T]$:

$$\int_0^T dt g_m(t) g_n(t) = \delta_{mn}. \quad (22)$$

In our calculations, two basis sets have been used: a sine basis:

$$g_n(t) = \sqrt{\frac{2}{T}} \sin\left(\frac{\pi}{T} nt\right), \quad n = 1 \dots N, \quad (23)$$

or a normal Fourier basis:

$$g_n(t) = \begin{cases} \sqrt{\frac{2}{T}} \cos\left(\frac{2\pi}{T} nt\right), & n = 1, \dots, \frac{N}{2}, \\ \sqrt{\frac{2}{T}} \sin\left(\frac{2\pi}{T} \left(n - \frac{N}{2}\right)t\right), & n = \left(\frac{N}{2} + 1\right), \dots, N. \end{cases} \quad (24)$$

The representation in these basis sets has the advantage that spectral constraints can be automatically enforced: the maximum frequency is given by the choice of N , and we will not include the zero-frequency component, in order to satisfy condition (18).

We can directly choose the basis set expansion coefficients as control parameters, or else constrain further the search space to meet other physical or experimental requirements, by defining the coefficients as functions of a reduced set of parameters: $\tilde{\epsilon}_n = \tilde{\epsilon}_n[u]$. Our choices have been the following:

- A *constrained sine series*. The sine series, Eq. (23) automatically fulfills the condition given by Eq. (19). To meet condition (18), however, the following relation would have to be fulfilled:

$$\sum_{m=0}^{N/2-1} \frac{\tilde{\epsilon}_{(2m+1)}}{(2m+1)} = 0. \quad (25)$$

For some of the cases presented below, we also enforced a fixed fluence. As function of any orthonormal basis set coefficients, the fluence is given by:

$$\mathcal{F}[\tilde{\epsilon}] = \sum_{n=1}^N \tilde{\epsilon}_n^2. \quad (26)$$

Setting the fluence to a predefined value \mathcal{F}_0 amounts to requiring the vector $\tilde{\epsilon}$ to belong to a hypersphere. We may then transform $\tilde{\epsilon}$ into hyperspherical coordinates; the $N - 1$ angles θ_j will span the new search space, of one dimension less.

- A *constrained Fourier series*. If the zero-th frequency is left out, a Fourier series, Eq. (24), automatically fulfills condition (18). Condition (19) is met if:

$$\tilde{\epsilon}_1 = - \sum_{n=2}^{N/2} \tilde{\epsilon}_n. \quad (27)$$

To fulfill this condition, a first parameter transformation can be defined by

$$\tilde{\epsilon}_1 = - \sum_{n=1}^{N/2-1} \alpha_n, \quad (28)$$

$$\tilde{\epsilon}_{(n+1)} =: \alpha_n, \quad n = 1, \dots, (N - 1).$$

In terms of the new coordinates, it is trivial to see that the fluence is given by a bilinear expression:

$$\mathcal{F}[\alpha] = \alpha^T S \alpha, \quad (29)$$

for a $(N - 1) \times (N - 1)$ symmetric matrix S . It can be diagonalized by performing a new change of coordinates based on an orthonormal matrix U :

$$U^T S U = \begin{pmatrix} s_1 & & 0 \\ & \ddots & \\ 0 & & s_{(N-1)} \end{pmatrix} \quad (30)$$

and if we now define a final change of coordinates in the form:

$$\beta = L U^T \alpha, \quad (31)$$

where:

$$L := \begin{pmatrix} \sqrt{s_1} & & 0 \\ & \ddots & \\ 0 & & \sqrt{s_{(N-1)}} \end{pmatrix} \quad (32)$$

then the fluence has the simple form:

$$\mathcal{F}[\beta] = \sum_{n=1}^{N-1} \beta_n^2. \quad (33)$$

Once we have this form, in order to fix the fluence to a predefined value \mathcal{F}_0 one can once again make a coordinate transformation to hyperspherical coordinates, and use the $N - 2$ angles as search space.

2.3.2. Optimization algorithms

There are two broad families of optimization algorithms: gradient-free and gradient-based schemes. We will utilize both in the application presented below.

Gradient-free. In experimental control experiments, the gradient of the merit function is seldom available, and the most used gradient-free algorithms belong to the “evolutionary” or “genetic” families. These are specifically designed for search spaces with large number of dimensions, typically discrete [46,47].

However, in our code we have opted for two different schemes, which are sufficient for a moderate number of continuous degrees of freedom: the classic simplex algorithm of Nelder and Mead [48], and Powell’s NEWUOA algorithm [49], newer and more efficient.

Gradient-based. If the control function is described in any parameterized representation, then we have used a standard conjugate gradient algorithm, the Broyden–Fletcher–Goldfarb–Shanno variant [50].

However, if the control function is represented directly in real time (which usually implies a large number of degrees of freedom), a number of different algorithms that were specifically developed within the field of QOCT (or adapted to it) have been proposed. These can provide very fast convergence, if they are applicable. In particular, very successful techniques are the Krotov method [51] and the monotonically convergent techniques proposed by Zhu and collaborators [52,53]. In some of the examples given below, we will use one of these latter techniques [52].

Note that if the control function is constrained in any way (as it happens for our laser fields), there exist local maxima or “traps” in the control landscape [54]. Thus, we will find, no matter what optimization algorithm is used, these local maxima when the searches are performed. This will be manifested by the initial-pulse dependence of the final results.

3. Results: control targets based on the forces

During the breaking of a bond, the forces that act on the two separating nuclei should have more or less opposite directions in space, i.e., a naive but reasonable attempt to define a bond-breaking target is to do it in terms of the forces: one can attempt the

maximization of the force difference between the nuclei that must be separated, and the minimization of the forces between the nuclei remaining in each fragment. In this section we describe a first attempt in which the target includes the value of the forces only at the end of the action of the pulse – it is, therefore, a static target.

We will assume that the laser pulse is short, so that during its action the nuclei do not move significantly; therefore the optimization calculations will be performed with frozen nuclei. The idea is that the pulse should be able to place the electrons on a dissociating state. Later, the optimized pulse will be tested without the fixed nuclei restriction. In this “bond breaking test run”, therefore, the calculation was based on the mixed quantum–classical description described earlier.

We used a simple 1D model of a triatomic Hydrogen molecule (see Fig. 1), with two non-interacting electrons. The electron–nucleus interaction is modelled with a soft Coulomb potential:

$$v_{\text{nuc}}(x, x_i) = -\frac{1}{\sqrt{(x - x_i)^2 + 1}}, \quad (34)$$

where x is the electronic coordinate, and x_i is the nuclear position of nucleus i . Since we have two independent electrons evolving in a spin-independent Hamiltonian, we can assume the system to be permanently in a singlet state: both the two electrons occupy the same orbital Ψ , which is initially the ground state. It evolves governed by the Hamiltonian:

$$\hat{H}[\epsilon, t] = -\frac{1}{2}\partial_x^2 + \hat{x}\epsilon(t) + \sum_{i=1}^3 v_{\text{nuc}}(\hat{x}, x_i). \quad (35)$$

The temporal dependence of the laser field is determined by the function $\epsilon(t)$, for which we will consider in this case a real time representation.

The target functional F will be divided into the object that truly needs to be optimized, J_1 , and a penalty function J_2 :

$$F[\Psi, \epsilon] = J_1[\Psi] + J_2[\epsilon]. \quad (36)$$

The task of J_2 is to prevent unphysically large fluences:

$$J_2[\epsilon] = -\alpha \mathcal{F}[\epsilon] = -\alpha \int_0^T dt \epsilon^2(t). \quad (37)$$

The constant α is the “penalty factor”; it is positive, and it regulates the weight that is put in the low fluence condition.

The definition that we choose for J_1 is:

$$J_1[\Psi] = (F_2[\Psi(T)] - F_3[\Psi(T)]) - |F_1[\Psi(T)] - F_2[\Psi(T)]|^2, \quad (38)$$

where $F_i[\Psi(T)]$ is the force acting on nucleus i at the end of the pulse action, and is given by:

$$\begin{aligned} F_i[\Psi(T)] &= -2\langle \Psi(T) | \partial_{x_i} v_{\text{nuc}}(\hat{x}, x_i) | \Psi(T) \rangle + \sum_{j \neq i} \frac{Z_i Z_j (x_i - x_j)}{|x_i - x_j|^3} \\ &= \int dx n(x, T) \partial_x v_{\text{nuc}}(\hat{x}, x_i) + \sum_{j \neq i} \frac{Z_i Z_j (x_i - x_j)}{|x_i - x_j|^3}. \end{aligned} \quad (39)$$

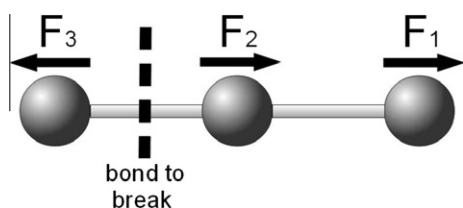


Fig. 1. Sketch of the 1D test model. The direction of the arrows indicates the direction of the force optimization.

This definition of J_1 attempts to maximize the force difference between nucleus 2 and 3, and minimize the force between nucleus 1 and 2. There are some parameters in this expressions that one can experiment with: the second term in the right hand side of Eq. (38) could be multiplied by a weighting factor, or the square could be eliminated or changed by other exponent. Note that this type of force target is an explicit functional of the density $n(x, T) = 2|\Psi(x, T)|^2$ – this is not so relevant in the independent electrons approximation taken in this case, but it is in the Kohn–Sham case that will be discussed later.

We must now adapt the QOCT Eqs. (1), (2), (11), (12) and (10) to this particular case. Schrödinger’s equation, together with its initial condition, (1) and (2), obviously do not change. The evolution equation for the auxiliary χ wave function is in this case given by:

$$i\frac{\partial \chi[\epsilon]}{\partial t}(x, t) = \hat{H}[\epsilon, t]\chi[\epsilon](x, t), \quad (40)$$

$$\chi[\epsilon](x, T) = O(x)\Psi(x, T), \quad (41)$$

where

$$\begin{aligned} O(x) &= \partial_x [v_{\text{nuc}}(x, x_2) - v_{\text{nuc}}(x, x_3)] - 2[F_1[\Psi(T)] \\ &\quad - F_2[\Psi(T)]]\partial_x [v_{\text{nuc}}(x, x_1) - v_{\text{nuc}}(x, x_2)]. \end{aligned} \quad (42)$$

Finally, Eq. (10) takes now the form:

$$\frac{\delta G}{\delta \epsilon(t)} = -2\alpha \epsilon(t) + 2\text{Im}\langle \chi[\epsilon](t) | \hat{x} | \Psi[\epsilon](t) \rangle. \quad (43)$$

At the maxima, this functional derivative is null, and therefore the solution field will be given by:

$$\epsilon(t) = \frac{1}{\alpha} \text{Im}\langle \chi[\epsilon](t) | \hat{x} | \Psi[\epsilon](t) \rangle. \quad (44)$$

In order to solve these equations, we chose the algorithm of Zhu and Rabitz [53]. This is a strictly monotonically convergent algorithm, as long as the target functional has the form of an expectation value, a condition that does not hold in our case. The algorithm requires an initial guess, which is then iteratively improved; we chose a sine wave with sine-shaped envelope (see Fig. 2):

$$\epsilon^{(0)}(t) = A_0 \sin\left(\frac{\pi}{T}t\right) \sin(\omega_0 t). \quad (45)$$

We used a laser pulse duration of $T = 400$ a.u. and an amplitude of $A_0 = 7 \cdot 10^{-2}$ a.u. We tested several frequencies for the initial field: $\omega_0 = (1, 2, \dots, 9) \cdot 10^{-2}$ a.u. (note that the final yield will depend on the choice of the initial guess).

We found that convergence is by no means guaranteed – only 3 of the 9 optimization runs showed a convergent behavior. Furthermore we observe that the convergence is not monotonic. This is demonstrated in Fig. 2 where we show, on the left panel, the convergence history for the case $\omega_0 = 4 \cdot 10^{-2}$ a.u. (all other cases were qualitatively similar). The right panel shows the initial and the converged laser pulse.

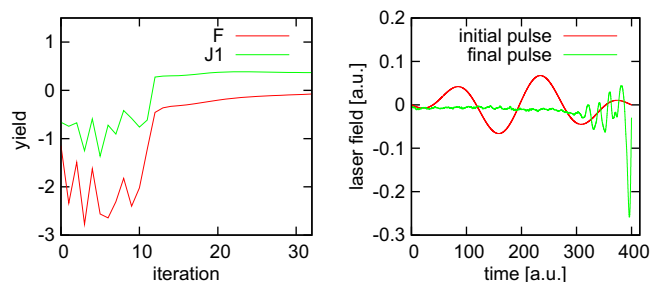


Fig. 2. Left: Convergence plot of the optimization run. Right: Initial and optimized laser pulses. The optimized pulse corresponds to iteration step 30.

We use the latter to check whether or not the bond breaks; we let evolve the system for 1000 a.u. (i.e., also after the pulse vanishes) with moving nuclei. Fig. 3 displays the forces and positions of the three nuclei during this process. We first observe that the forces obtained in the optimization run are not identical to the forces computed during this bond-breaking test run, since in this case the nuclei have been free to move during the short laser pulse. However, the differences were small, which validated (for this particular case) our static nuclei approximation. A second important observation is that the amplitudes of the force oscillations before and after the end of the pulse were of the order of, and even larger than, the optimized forces at the end of the pulse.

In Fig. 3 (right), we observe that we got a complete atomization of the test model in this run – which is not the objective. This negative result was typical of all runs: Either the test model was still bound and the nuclei just oscillated around their equilibrium positions for $t > 400$ a.u., or we got full atomization, as in the case presented. This latter case was triggered by a strong electronic ionization.

In view of the strong force oscillations observed, we may conclude that the main reason for this negative outcome is the time-independent character of our control target: the forces have a strong oscillatory character, and controlling them at a single moment in time does not suffice. This consideration leads naturally to the subject of the next section: the definition of the control targets in terms of the full history of the forces – their integrated values, or in other words, the momenta.

4. Results: control targets based on the momenta

In this section, we explore the option of defining the target functional in terms of the momenta of the nuclei at the end of the pulse. For this purpose, we used the same 1D model defined in the previous chapter.

The momenta are nothing else than the integrated forces:

$$p_i[\Psi] = \int_0^T d\tau F_i[\Psi(\tau)], \quad (46)$$

and the definition of the target functional F is simply done by replacing forces by momenta:

$$J_1[\Psi] = (p_2[\Psi] - p_3[\Psi]) - |p_1[\Psi] - p_2[\Psi]|^2. \quad (47)$$

Qualitatively, however, the problem changes, since $p_i[\Psi]$ are functionals of the full evolution of the system, i.e. we confront a time-dependent target. The three cases presented below differ in the manner in which the laser field is defined or restricted, and on the optimization algorithm.

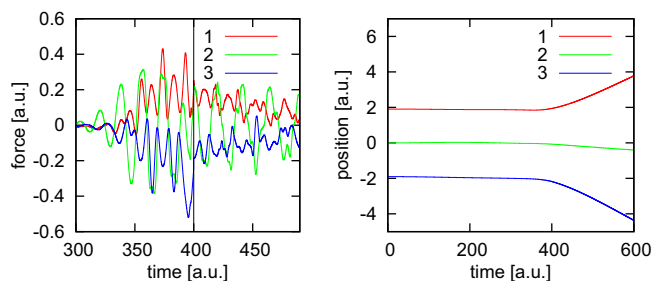


Fig. 3. Left: Forces on each nucleus during the bond breaking test run. The vertical black line indicates the end of the laser pulse. Right: Position of the nuclei during the bond breaking test run.

4.1. Gradient free optimization algorithm with fixed nuclei

In this first case, we used a parameterized representation for the control function (the electric field), in particular the constrained sine series (see Section 2.3.1): the search space is spanned by a set of hyperspherical angles $\theta = \{\theta_j\}$, and therefore the fluence is constant (making unnecessary the introduction of a penalty function J_2).

We test now a gradient-free procedure for the maximization of the function $G[\theta] = F[\Psi[\theta], \theta] = J_1[\Psi[\theta]]$, in particular the “downhill simplex” method from Nelder and Mead [48]. Each function evaluation amounts to one forward propagation (the backwards propagations are in this case unnecessary). As in the previous section, we used very short pulses and assumed the fixed-nuclei approximation during the pulse action. The optimization runs were followed by the corresponding “bond-breaking test runs”, in which the nuclei are allowed to move to check that the molecule breaks in the intended way.

As an initial guess for the pulse, we used, once again:

$$\epsilon^{(0)}(t) = A_0 \sin\left(\frac{\pi}{T}t\right) \sin(\omega_0 t). \quad (48)$$

We performed several calculations with varying values of ω_0 : $\omega_0 = (4 \dots 19) \cdot 10^{-2}$ a.u. The amplitude A_0 is adjusted so that all optimizations are performed with the same (constant) fluence. The propagating time was chosen to be $T = 200$ a.u. All functions were then expanded in a sine Fourier series, with frequencies $\omega_n = \frac{\pi}{T}n$ for $n = 1, 2, \dots, 12$. This means 11 degrees of freedom for the search space, once the transformation to hyperspherical coordinates was done.

All optimizations converged, and of those, half of them led to the sought bond destruction. We display results for one of the runs ($\omega_0 = 19 \cdot 10^{-2}$ a.u.), since all of them were qualitatively similar. Fig. 4 (left) shows the convergence history of F . The right side shows the initial and the optimized laser pulse (iteration step 100). It is clearly visible that this optimized pulse does not contain very high frequency components, compared to the pulse obtained

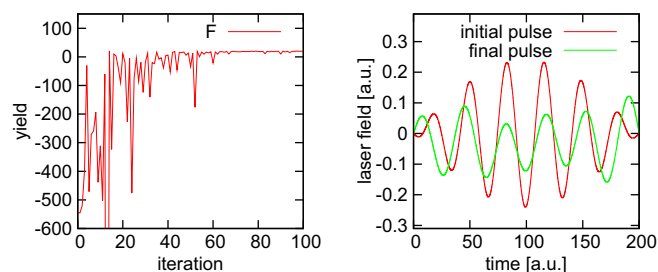


Fig. 4. Left: Convergence plot of the gradient-free optimization. Right: Initial and optimized laser pulses.

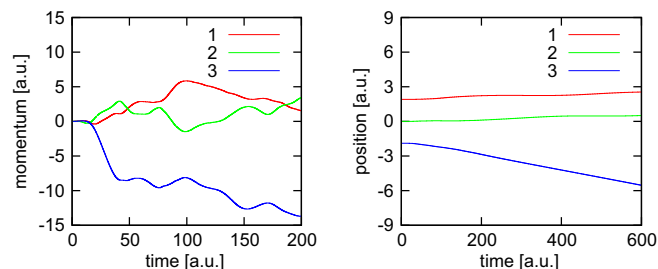


Fig. 5. Left: Momentum of each nucleus during the bond breaking test run. Right: Positions of the nuclei during the bond breaking test run.

in the forces-based optimization. This is due to the natural frequency cut-off imposed by the parameterization.

The left plot of Fig. 5 displays the momenta of the nuclei during the bond breaking test run. It is noteworthy that the momenta did not significantly oscillate for $t < 200$ a.u., as observed for the forces. The right plot, in turn, shows the coordinates of the nuclei during the bond breaking test run. It is clear that the intended goal was achieved: nucleus 3 dissociates from nucleus 1 and 2, that stay bound.

Despite the successes, the nuclear movement was not completely negligible during the action of the laser pulse. This can already be seen in the right panel of Fig. 5. In order to further study the influence of the nuclear movement, we performed runs with different pulse durations ($T = 100$ a.u. and $T = 400$ a.u.). The result is that for 100 a.u. many runs succeeded, while for 400 a.u. no run did. We may conclude that (1) constructing the control target functional in terms of the momenta of the nuclei is an appropriate approach to the problem of selective bond cleavage, but (2) the movement of the nuclei is, in general, not negligible when performing the optimization, unless the laser pulses are very short.

4.2. Gradient free optimization algorithm with moving nuclei

The natural next step is therefore to include the ionic motion during the optimization runs, in order to allow for larger pulse durations. We have attempted this using exactly the same model and target definition as in the previous section. The only difference is that, during the action of the pulse, the dynamic variables include not only the electronic orbital, but also the nuclear coordinates and momenta.

The laser pulse was represented in the same way as in the previous section: the set of hyperspherical angles that describe the fixed-norm (i.e. fixed fluence) coefficients of a sine series expansion. We tested, for these runs, in addition to the previously used downhill simplex scheme, a new gradient-free optimization algorithm: the NEWUOA [49] scheme. It is based on the construction of a higher order polynomial approximation to the function that needs to be optimized.

We used a total pulse length of $T = 400$ a.u., larger than in the previous case, in order to make the nuclear movement clearly non-negligible. The sine series expansion contained in this case 14 components, making the parameter space of 13 degrees of freedom. Several initial guesses of the form (48) were tried, with $\omega_0 = (3 \dots 9) \cdot 10^{-2}$ a.u. Each initial pulse was then optimized with the two maximization algorithms. We observed a much faster convergence (roughly double) with the NEWUOA algorithm. All tests, no matter what maximization algorithm was used, were successful: the optimized pulse led to the breaking of the selected bond. We describe the results obtained for the case $\omega_0 = 6 \cdot 10^{-2}$ a.u. (since all other cases showed a similar behavior).

The left plot of Fig. 6 compares both optimization algorithms. Clearly, the NEWUOA algorithm finds the maximum much faster. The right plot compares the optimized laser pulses. Here we see that the two algorithms found different local maxima – even if both achieved the attempted goal: the breaking of the selected bond.

The left plot of Fig. 7 displays the momenta of the nuclei during the bond breaking test run (performed with the laser pulse of iteration step 40 of the NEWUOA optimization). The right plot displays, in turn, the coordinates. The selected bond is broken quickly. We note that a certain degree of ionization occurred in all runs (the final charges oscillated between 1.1 and 2.0 a.u.) In all cases, most of the charge remained in the dimer fragment, permitting its stability. We can conclude that the inclusion of the movement of the nuclei in the optimization runs solves the prob-

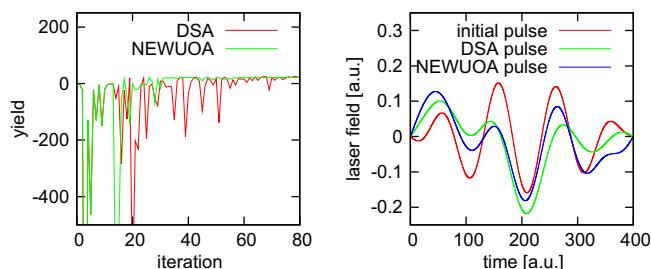


Fig. 6. Left: Convergence plot for the two different optimization algorithms. DSA stands for downhill simplex algorithm. Right: Initial and final laser pulse, for both the NEWUOA and the downhill simplex algorithms.

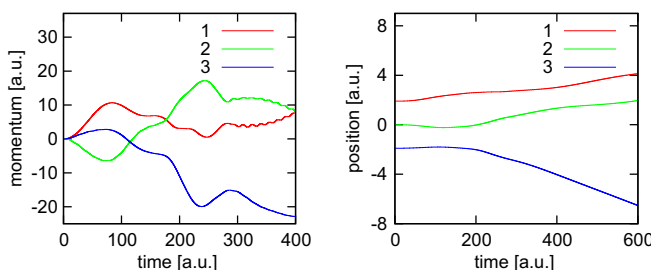


Fig. 7. Left: Momentum of each nucleus during the bond breaking test. Right: Nuclear coordinates, for the same calculation.

lems found in the previous section, when the pulse durations are not very short.

4.3. CG optimization for fixed nuclei

A target constructed in terms of the momenta can also be handled with a gradient based algorithm, for which the QOCT equations are needed. This subsection describes such calculation for the same model used in the previous two subsections. Note, however, that the QOCT equations presented above are valid for a quantum system, not for a mixed quantum–classical one. Therefore, the nuclei must be frozen during the optimization, and in consequence we are restricted once again to short pulses ($T = 200$ a.u., a case for which we saw that the frozen nuclei approximation is justified).

The laser pulse was represented by the Fourier series (24), and further constraints (constant fluence, zero average field) were then implemented as described in Section 2.3.1 – the parameter set is then a set of hyperspherical angles θ . We slightly changed the definition of the target:

$$J_1[\Psi] = (p_2[\Psi] - p_3[\Psi]) - 10|p_1[\Psi] - p_2[\Psi]|, \quad (49)$$

in order to have linear dependence with respect to the momenta for the two terms in the right hand side, since we observed that this choice usually provides better convergence. The factor “10” can also be changed, and regulates the weight that is placed on the minimization of the momenta difference between those atoms that must remain bound.

Due to the time-dependent nature of the target, Eq. (11) is now inhomogeneous, and the evolution of the auxiliary wave function χ is governed by the following equations:

$$i \frac{\partial \chi[\theta]}{\partial t}(x, t) = \hat{H}[\theta, t] \chi[\theta](x, t) - i \frac{\delta J_1}{\delta \Psi^*[\theta](x, t)}. \quad (50)$$

$$\chi[\theta](x, T) = 0. \quad (51)$$

The gradient $\nabla_\theta G[\theta]$ can be calculated by Eq. (9) [55]. This gradient can then be used to perform a conjugate gradients [50] optimization.

We performed a number of runs with this scheme, and the results did not differ qualitatively of the results obtained with the gradient-free algorithm: partial ionization, and successful bond-breaking in about half of the runs. The purpose of these calculations was to make a comparison regarding the computational efficiency, and therefore we only show results corresponding to one run that was performed with identical parameters with both optimization schemes.

The left plot of Fig. 8 compares the convergence for the two methods. The NEWUOA algorithm reached the maximum after about 60 propagations, whereas the CG method just needed about 25 propagations. This was typical, in all runs, the NEWUOA method needed about twice the computing time to reach convergence. (note that in the CG case, each propagation corresponds to either a backwards or a forwards propagation, which require roughly the same computer time).

The right plot of Fig. 8 shows the optimized laser pulses for both methods. One can see that the two pulses look rather similar. Nevertheless, there are some small differences in the optimized pulses which became noticeable in the ionization of the system: while the electronic charge decreased to about 1.65 a.u. when irradiating the system with the pulse obtained with the CG optimization run, we got a decrease of the electronic charge to about 1.3 a.u. when the NEWUOA pulse was used.

We can conclude that a gradient-based technique such as CG is also applicable to this problem, and is even more efficient, despite the complications due to the necessity of backwards propagating an inhomogeneous Schrödinger-like equation. Unfortunately, the scheme cannot yet be applied to longer pulses in which the nuclei should be allowed to move. In those cases, the nuclear equations of motion must then be included, as well as the electronic quantum equation, in the OCT formalism. Work along these lines is in progress.

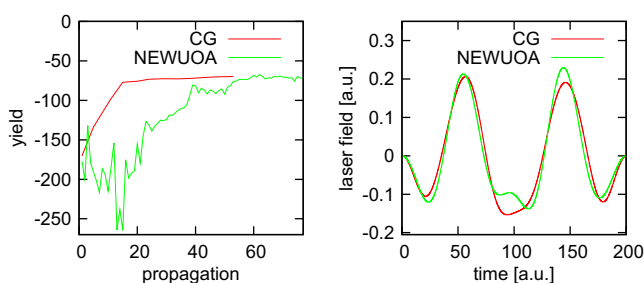


Fig. 8. Left: Comparison between the CG and NEWUOA optimization. Right: Comparison of the optimized laser pulses.

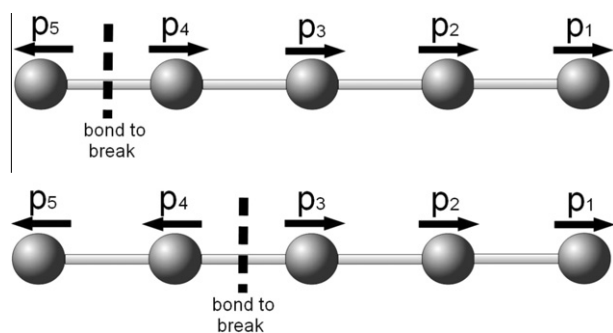


Fig. 9. Sketch of the 5-atomic 1D test model.

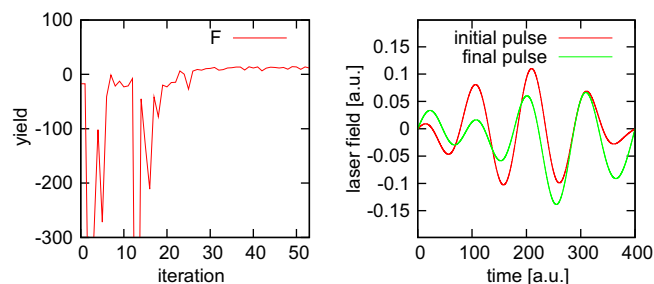


Fig. 10. Left: Convergence plot (NEWUOA algorithm) for the 4 + 1 chain bond breaking attempt. Right: Initial laser pulse and optimized laser pulse.

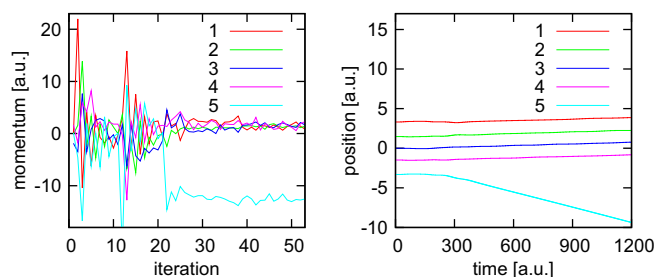


Fig. 11. Left: Momentum of each nucleus during the optimization run, for the 4 + 1 bond breaking attempt. Right: Coordinates of the nuclei during the bond breaking test run.

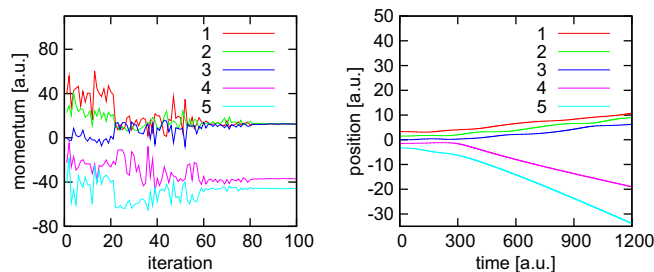


Fig. 12. Left: Momentum of each nucleus during one of the the 3 + 2 optimization runs. Right: Coordinates of the nuclei during the corresponding bond breaking test run.

5. Selective bond breaking of 1D chains

A more stringent test on the methodology consists of attempting to obtain different sized fragments in longer 1D atomic chains. We now show calculations of five equal mass atom chains, for which we attempt to break the chain into either 4 + 1 or 3 + 2 fragments (see Fig. 9). The chain consists of 5 Hydrogen nuclei; as in previous section, they interact with the electrons through a soft Coulomb potential. We place four non-interacting electrons; this means that instead of one single wave function Ψ , we now have two doubly occupied orbitals ψ_1, ψ_2 . The construction of the control target was based on the same ideas discussed earlier: maximizing or minimizing momenta differences. For example, for the 4 + 1 cleavage attempt:

$$J_1[\psi_1, \psi_2] = (p_4[\psi_1, \psi_2] - p_5[\psi_1, \psi_2]) - 10 \sum_{i=1}^3 |p_i[\psi_1, \psi_2] - p_{i+1}[\psi_1, \psi_2]|, \quad (52)$$

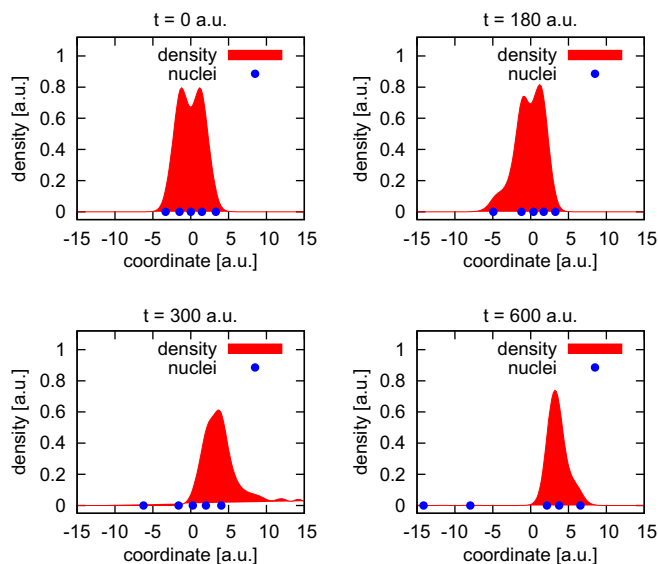


Fig. 13. Electronic density, and nuclear coordinates at different times during the bond breaking test run for one of the 3 + 2 chain cleavage attempt. The laser pulse duration was $T = 400$ a.u.

whereas for the 3 + 2 case:

$$J_1[\psi_1, \psi_2] = (p_3[\psi_1, \psi_2] - p_4[\psi_1, \psi_2]) - 10 \sum_{i=1, i \neq 3}^4 |p_i[\psi_1, \psi_2] - p_{i+1}[\psi_1, \psi_2]|. \quad (53)$$

In this case, we considered moving nuclei and we applied a gradient free optimization by making use of the NEWUOA algorithm. Again, we used (48) as initial pulse with a pulse duration of $T = 400$ a.u. The pulse was represented by the constrained sine series and in this case we restricted the parameter search space to 11 hyperspherical angles. The following initial parameters have been tested: $\omega_0 = (3, \dots, 6) \cdot 10^{-2}$ a.u.

For the 4 + 1 bond breaking attempt, almost all runs were successful (for two of them the field was too weak to remove any nucleus). There was no ionization, and all the electronic charge remained by the 4 nuclei, while one proton separated away. The plots in Figs. 10 and 11 correspond to the run with $\omega_0 = 6 \cdot 10^{-2}$ a.u. The other successful runs were qualitatively similar.

For the 3 + 2 bond breaking attempt, the results were different. The optimization converged for all runs. However, only 2 of 10 bond breaking test runs were successful. In the other cases, we either obtained no ionization and unwanted 4 + 1 separation like in the previous case, or else substantial ionization and Coulomb explosion of the full system.

The plots shown in Fig. 12 correspond to one successful run, namely that with $\omega_0 = 6 \cdot 10^{-2}$ a.u. Fig. 13 shows the corresponding electronic density distribution and the coordinates of the nuclei at different times. At $t = 300$ a.u., an ionization of the system is observed. In fact, we found that a certain ionization was needed to remove the two nuclei. In this particular case, the electronic charge decreased from 4.0 a.u. to 2.3 a.u. during the laser pulse. This ionization necessarily implied an unwanted effect, namely that nucleus 4 and 5 were not bound to each other anymore after removing them (see plot for $t = 600$ a.u.).

Therefore, for this particular choice of model, search space and algorithm, the optimization runs did not succeed. However, we expect that this can be cured in a number of ways, since there is a large freedom to be explored regarding the definition of the target functional. For example, the introduction of the ionization in the definition (prevention or encouragement of ionization) could help to avoid undesired effects caused by it. As a final remark, we men-

tion that we performed further tests with atomic chains with different masses [55]; in those cases, it was found that the momenta should be substituted by the velocities in order to obtain better results.

6. H_3^+

The next example is a more realistic molecular description: a 3D calculation for the H_3^+ molecule, considering interacting electrons. Fig. 14 shows the geometry of this molecule [56]; it has an equilateral shape with an edge length of 1.64 a.u.

The two electrons were treated with TDDFT and the exchange–correlation potential was approximated by the ALDA. The motion of the nuclei was treated classically. The electron–nucleus interaction was described by pseudo-potentials – in this case, obviously, the pseudo-potentials are not used to remove any core electrons, but as a means to smooth the Coulomb singularity.

We tried to obtain a laser pulse which removes one particular nucleus, leaving a bound Hydrogen molecule, by making use of the same kind of momentum target described above. Fig. 14 shows the directions in which the momenta were optimized; the control target is defined as:

$$J_1[\Psi] = \vec{n} \cdot (\vec{p}_1[\Psi] - \vec{p}_2[\Psi]) - |\vec{p}_2[\Psi] - \vec{p}_3[\Psi]|, \quad (54)$$

where Ψ is the Kohn–Sham orbital occupied by the two electrons. Note that this functional is an explicit functional of the density.

We used the gradient free NEWUOA algorithm for the optimization, and we did not neglect the nuclear movement. The initial pulse was chosen to be in the form given by Eq. (48), and the pulse duration was $T = 400$ a.u. In this 3D case, we also have to specify the laser polarization, which was chosen parallel to \vec{n} . The param-

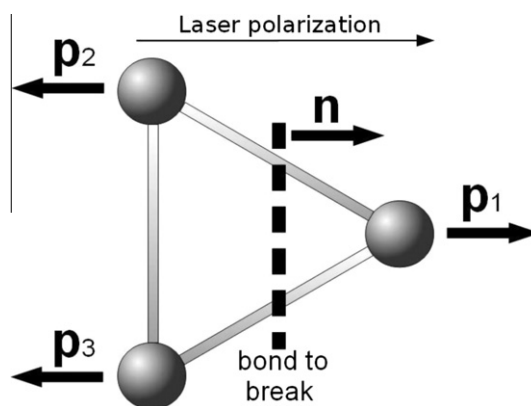


Fig. 14. Sketch of H_3^+ . The dashed line indicates the separation plane, where the molecule ought to be broken. The normal vector \vec{n} lies in the molecular plane and is perpendicular to the separation plane. The laser polarization is parallel to \vec{n} , and the direction of the optimized momenta \vec{p}_i is parallel to \vec{n} as well.

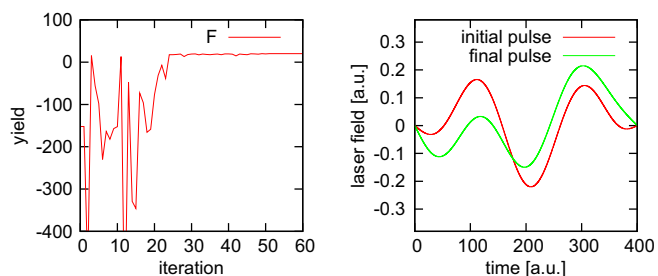


Fig. 15. Left: Convergence plot for the H_3^+ example. Right: Initial and optimized (corresponding to iteration step 40) laser pulses.

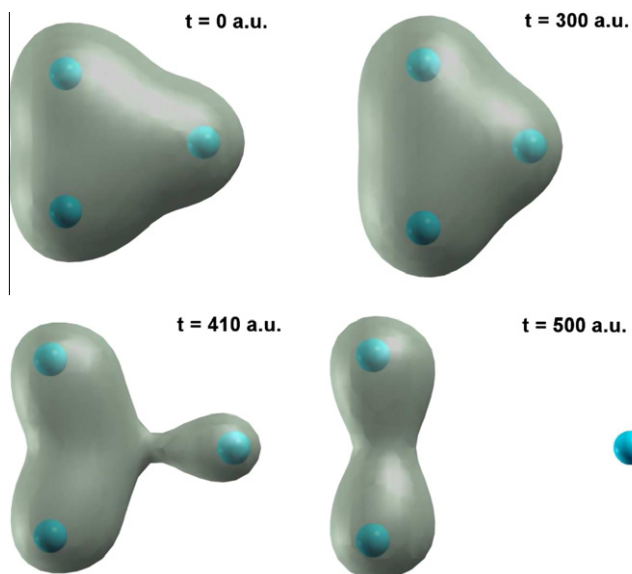


Fig. 16. Isosurface plot of the electronic density and the corresponding positions of the nuclei during the bond breaking test run at different times. The isosurface was plotted at a density of 0.07 a.u. The laser pulse duration was $T = 400$ a.u.

eterization used to represent this laser pulses was the constrained sine series.

We display in Figs. 15 and 16 the results of one typical optimization run, corresponding to an initial guess with $\omega_0 = 3 \cdot 10^{-2}$ a.u. It can be seen how the convergence is rather fast, and the obtained pulse cuts the molecule in the desired way. The electronic charge decreased from 2.0 a.u. to around 1.5 a.u.

7. CH_2NH_2^+

A more complex molecule is CH_2NH_2^+ , the “methaniminium cation”. The loss of H^+ as well as H_2 from CH_2NH_2^+ has been extensively investigated, both experimentally and theoretically [57,58]. Our goal was the former, the removal of one of the protons, the one that binds to the Nitrogen nucleus (this process leads to CH_2NH , “methylenimine”, see Fig. 17).

We started our calculations from the ground state in which CH_2NH_2^+ has a planar shape (see Fig. 17). Then, the simulation of the molecule dynamics of CH_2NH_2^+ was performed similarly to that of H_3^+ , with the described mixed quantum classical description on

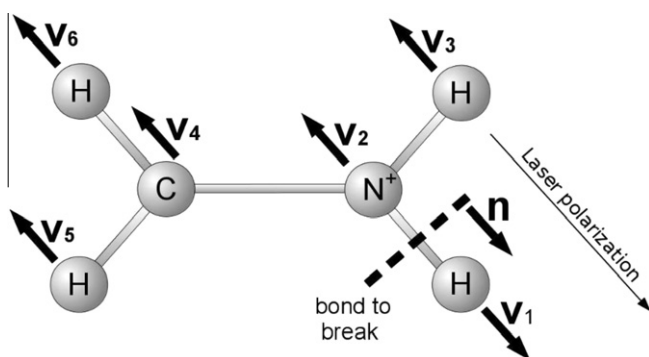


Fig. 17. Sketch of CH_2NH_2^+ . The dashed line indicates the separation plane, where the molecule ought to be broken. The normal vector \vec{n} lies in the molecular plane and is perpendicular to the separation plane. The laser polarization as well as the directions in which the velocities \vec{v}_i were optimized are parallel to \vec{n} .

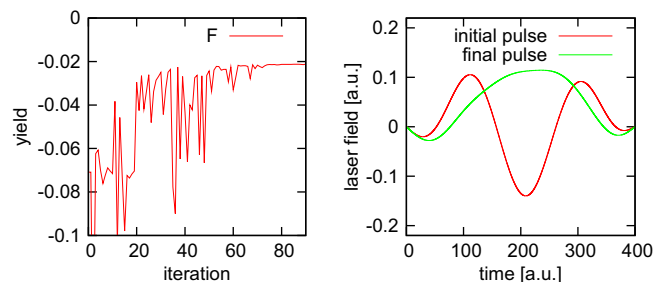


Fig. 18. Left: Convergence history of the CH_2NH_2^+ dissociation attempt, for which the NEWUOA algorithm was used. Right: Initial and optimized laser pulses for this case.

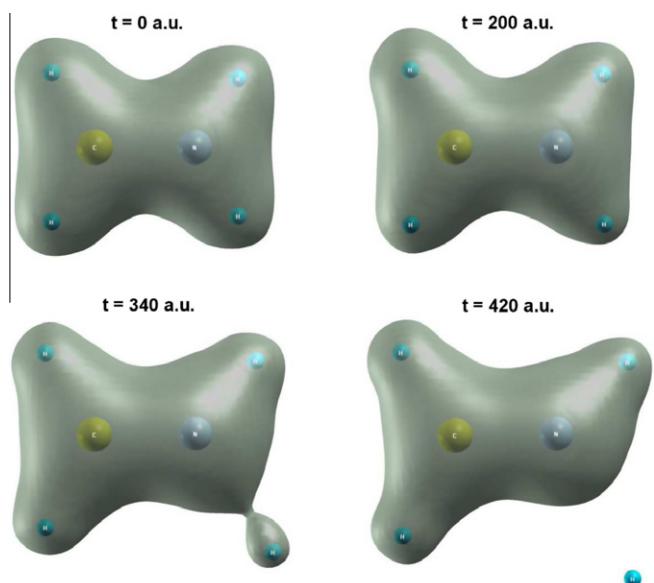


Fig. 19. Isosurface plot of the electronic density and the corresponding positions of the nuclei. The isosurface value of the density was 0.045 a.u. The laser pulse duration was $T = 400$ a.u.

top of TDDFT. The exchange–correlation potential was approximated by the ALDA. The potentials of the nuclei were described by pseudo-potentials (in this case, this means that the two core electrons of C and N are frozen).

Since we are now working with a molecule that contains nuclei with different masses, we will define our target in terms of the velocities, instead of using the momenta (the nuclear labels are defined in Fig. 17):

$$J_1[n] = \vec{n} \cdot (\vec{v}_1[n] - \vec{v}_2[n]) - 10 \sum_{i=3}^6 |\vec{v}_2[n] - \vec{v}_i[n]|. \quad (55)$$

Again, this target functional is an explicit functional of the electronic density; this is important conceptually since we are using TDDFT, where the many-body wave function is not easily accessible. In the previous equation, we have show explicitly this functional dependence on the density. The normal vector \vec{n} as well as the laser polarization direction were chosen to be parallel to the bond axis between the Nitrogen nucleus and the Hydrogen nucleus.

Again, we used the NEWUOA algorithm and the form given in Eq. (48) for the initial pulse; the pulse duration was $T = 400$ a.u. The electric field was expanded in a sine series, and the constrained sine series parameterization was used once again (this time, with 10 degrees of freedom). As usual, we performed optimi-

zations with a number of initial guesses, varying frequencies and amplitudes (but keeping the fluence constant). Only one of the attempts was successful, namely that with the initial frequency $\omega_0 = 3 \cdot 10^{-2}$ a.u. The plots in Figs. 18 and 19 correspond to this successful run. The electronic charge decreased from 12.0 a.u. to 11.0 a.u. in this run. In the other cases, the amplitudes of the optimized electric fields were either too small or too large: too small electric fields merely led to oscillations of the nuclei around their equilibrium positions, whereas too large fields, on the other hand, caused high ionization, which led to unintended dissociations.

8. Conclusions

This work addresses the challenge of selective photochemistry by means of high intensity shaped ultra-short laser pulses. The rapid experimental advances in forming laser pulses of almost arbitrary shape call for reliable theoretical tools to predict optimal pulse shapes for certain predefined tasks. To achieve this goal, our basic strategy is to combine the mathematical framework of optimal control theory with a mixed quantum–classical description of the molecular degrees of freedom: The electronic response of the system is described from first principles using TDDFT while the nuclear degrees of freedom are governed by classical equations of motion with Ehrenfest forces that mediate the coupling to the electronic degrees of freedom.

The task that the laser pulse is supposed to perform has to be formulated in terms of a “control target” or “target functional” to be maximized by the optimal pulse. Usually a given task, like breaking a selected bond, can be formulated in terms of several possible target functionals. This is where mathematical intuition and physical creativity come into play. The mixed quantum–classical description employed in this work lends itself to formulating the target functional for bond breaking in terms of the classical nuclear degrees of freedom. We have explored target functionals based on the classical forces acting on the nuclei, either considering their value at the end of the laser pulse, or considering their integrated value over the full propagation. This latter case means that the target functional depends on the nuclear momenta at the end of the pulse. The results show a clear superiority of the momentum-based target functional. This makes perfect sense because the oscillatory character of the forces makes their value at a single point in time less relevant than the integrated values. For molecules with different nuclei, it turns out to be better to define the targets in terms of the nuclear velocities rather than the momenta.

After defining the microscopic description of the system and choosing the control target functional, there is still ample freedom in the choice of optimization algorithms. We have utilized two fundamentally different types: gradient-free and gradient based algorithms. The latter were found, not surprisingly, to perform better. They require, however, a more elaborate theory, since the gradient (or functional derivative) calculation involves the backwards propagation of an auxiliary wave function which is particularly complicated when the basic equation of motion is non-linear (like in TDDFT) [33].

The calculations presented for H_3^+ and for CH_2NH_2^+ clearly demonstrate that selective bond breaking can be achieved with the target functionals and optimization algorithms developed in this work. An immediate task for the future will be the application to larger molecules. Furthermore, one may consider the definition of refined target functionals in order to prevent that the removed fragments break apart later. For example, a term that enhances the electronic charge localization between the nuclei of the removed fragments could be included in the target functional. Work along these lines is in progress.

Acknowledgements

This work was partially supported by the Deutsche Forschungsgemeinschaft within the SFB 658, and by the research project FIS2009-13364-C02-01 (MICINN, Spain).

References

- [1] T.H. Maiman, *Nature* 187 (4736) (1960) 493.
- [2] W.S.C. Chang, *Principles of Lasers and Optics*, Cambridge University Press, New York, 2005.
- [3] N. Bloembergen, A.H. Zewail, *The Journal of Physical Chemistry* 88 (23) (1984) 5459.
- [4] A.H. Zewail, *Physics Today* 33 (11) (1980) 27.
- [5] T. Elsaesser, W. Kaiser, *Annual Review of Physical Chemistry* 42 (1) (1991) 83.
- [6] P. Brumer, M. Shapiro, *Chemical Physics Letters* 126 (6) (1986) 541.
- [7] P. Brumer, M. Shapiro, *Faraday Discussions of the Chemical Society* 82 (1986) 177.
- [8] M. Shapiro, P. Brumer, *Principles of the Quantum Control of Molecular Processes*, Wiley, New York, 2003.
- [9] D.J. Tannor, S.A. Rice, *The Journal of Chemical Physics* 83 (10) (1985) 5013.
- [10] J. Herek, A. Materny, A. Zewail, *Chemical Physics Letters* 228 (1–3) (1994) 15.
- [11] U. Gaubatz, P. Rudecki, M. Becker, S. Schiemann, M. Klz, K. Bergmann, *Chemical Physics Letters* 149 (5–6) (1988) 463.
- [12] K. Ohmori, *Annual Review of Physical Chemistry* 60 (1) (2009) 487. PMID: 19335221..
- [13] H. Rabitz, *New Journal of Physics* 11 (10) (2009) 105030.
- [14] C. Brif, R. Chakrabarti, H. Rabitz, *New Journal of Physics* 12 (2010) 075008.
- [15] R.S. Judson, H. Rabitz, *Physical Review Letters* 68 (10) (1992) 1500.
- [16] C.J. Bardeen, V.V. Yakovlev, K.R. Wilson, S.D. Carpenter, P.M. Weber, W.S. Warren, *Chemical Physics Letters* 280 (1–2) (1997) 151.
- [17] A.M. Weiner, *Review of Scientific Instruments* 71 (5) (2000) 1929.
- [18] J. Werschnik, E.K.U. Gross, *Journal of Physics B: Atomic, Molecular and Optical Physics* 40 (2007) R175.
- [19] S. Shi, A. Woody, H. Rabitz, *The Journal of Chemical Physics* 88 (1988) 6870.
- [20] A.P. Peirce, M.A. Dahleh, H. Rabitz, *Physical Review A* 37 (1988) 4950.
- [21] R. Kosloff, S.A. Rice, P. Gaspard, S. Tersigni, D.J. Tannor, *Chemical Physics* 139 (1989) 201.
- [22] D.G. Luenberger, *Introduction to Dynamic Systems*, John Wiley & Sons, Inc., 1979.
- [23] D.G. Luenberger, *Optimization by Vector Space Methods*, John Wiley & Sons, Inc., 1969.
- [24] M. Protopapas, K.H. Keitel, P.L. Knight, *Reports of Progress in Physics* 60 (1997) 389.
- [25] T. Brabec, F. Krausz, *Reviews of Modern Physics* 72 (2000) 545.
- [26] A. Scrinzi, M.Y. Ivanov, R. Kienberger, D.M. Villeneuve, *Journal of Physics B: Atomic, Molecular and Optical Physics* 39 (2006) R1.
- [27] M. Mundt, D.J. Tannor, *New Journal of Physics* 11 (10) (2009) 105030.
- [28] A. Castro, E. Räsänen, A. Rubio, E.K.U. Gross, *EPL* 87 (2009) 53001.
- [29] E. Räsänen, A. Castro, J. Werschnik, A. Rubio, E.K.U. Gross, *Physical Review Letters* 98 (2007) 157404.
- [30] E. Räsänen, A. Castro, J. Werschnik, A. Rubio, E.K.U. Gross, *Physical Review B* 77 (2008) 065324.
- [31] M.A.L. Marques, C.A. Ullrich, F. Nogueira, A. Rubio, E.K.U. Gross (Eds.), *Time-Dependent Density Functional Theory*, Springer, Berlin, 2006.
- [32] E. Runge, E.K.U. Gross, *Physical Review Letters* 52 (12) (1984) 997.
- [33] A. Castro, J. Werschnik, E.K.U. Gross, Controlling the dynamics of many-electron systems from first principles: a marriage of optimal control and time-dependent density-functional theory. Available from: <arxiv:1009.2241v1>.
- [34] U. Saalman, R. Schmidt, *Zeitschrift für Physik D* 38 (1996) 153.
- [35] U. Saalman, R. Schmidt, *Physical Review Letters* 80 (1998) 3213.
- [36] E.K.U. Gross, J.F. Dobson, M. Petersilka, *Topics in Current Chemistry* 181: *Density Functional Theory II*, Springer, Berlin, 1996.
- [37] A. Castro, M.A.L. Marques, J.A. Alonso, G. Bertsch, A. Rubio, *The European Physical Journal D* 28 (2004) 211.
- [38] Y. Ohtsuki, G. Turinici, H. Rabitz, *The Journal of Chemical Physics* 120 (2004) 5509.
- [39] I. Serban, J. Werschnik, E.K.U. Gross, *Physical Review A* 71 (2005) 053810.
- [40] D.M. Ceperley, B.J. Alder, *Physical Review Letters* 45 (7) (1980) 566.
- [41] M.A.L. Marques, A. Castro, G.F. Bertsch, A. Rubio, *Computer Physics Communications* 151 (1) (2003) 60.
- [42] A. Castro, H. Appel, M. Oliveira, C.A. Rozzi, X. Andrade, F. Lorenzen, M.A.L. Marques, E.K.U. Gross, A. Rubio, *physica status solidi (b)* 243 (2006) 2465.
- [43] A. Castro, M.A.L. Marques, A. Rubio, *The Journal of Chemical Physics* 121 (8) (2004) 3425.
- [44] S. Chelkowski, A. Bandrauk, *Physical Review A* 71 (2005) 053815.
- [45] J. Werschnik, E.K.U. Gross, *Journal of Optics B: Quantum and Semiclassical Optics* 7 (2005) S300.
- [46] D.E. Goldberg, *Genetic Algorithms in Search, Optimization, and Machine Learning*, Addison-Wesley, Reading, 1993.
- [47] H.-P. Schwefel, *Evolution and Optimum Seeking*, Wiley, New York, 1995.
- [48] J.A. Nelder, R. Mead, *Computer Journal* 7 (1965) 308.
- [49] M.J.D. Powell, *Large Scale Nonlinear Optimization*, Springer, New York, 2004. pp. 255–297.

- [50] R. Fletcher, Practical Methods of Optimization, Wiley, New York, 2001.
- [51] J. Somló, V.A. Kazakov, D.J. Tannor, Chemical Physics 172 (1993) 85.
- [52] W.S. Zhu, J. Botina, H. Rabitz, The Journal of Chemical Physics 108 (1998) 1953.
- [53] W.S. Zhu, H. Rabitz, The Journal of Chemical Physics 109 (1998) 385.
- [54] H.A. Rabitz, M.M. Hsieh, C.M. Rosenthal, Science 303 (2004) 1998.
- [55] For more details, see K. Krieger, MSc thesis (Freie Universität Berlin, 2010).
- [56] N. Indriolo, T.R. Geballe, T. Oka, G.J. McCall, Astrophysical Journal 671 (2007) 1736.
- [57] T.H. Choi, S.T. Park, M.S. Kim, The Journal of Chemical Physics 114 (2001) 14.
- [58] G. Hvistendahl, E. Uggerud, Organic Mass Spectrometry 20 (1985) 541.